PHYSICAL REVIEW D **94,** 074012 (2016)

Excited bottom and bottom-strange mesons in the quark model

Qi-Fang Lü, Ting-Ting Pan, Yan-Yan Wang, En Wang, and De-Min Li*

Department of Physics, Zhengzhou University, Zhengzhou, Henan 450001, China

(Received 17 July 2016; published 6 October 2016)

In order to understand the possible $q\bar{q}$ quark-model assignments of the $B_J(5840)$ and $B_J(5960)$ recently reported by the LHCb Collaboration, we evaluate mass spectra, strong decays, and radiative decays of bottom and bottom-strange mesons in a nonrelativistic quark model. Comparing these predictions with the relevant experimental results, we suggest that the $B_J(5840)$ and $B_J(5960)$ can be identified as the $B(2^1S_0)$ and $B(1^3D_3)$, respectively, and the $B(5970)$ reported by the CDF Collaboration can be interpreted as the $B(2^3S_1)$ or $B(1^3D_3)$. Further precise measurements of the width, spin and decay modes of the $B(5970)$ are needed to distinguish these two assignments. These predictions of bottom and bottom-strange mesons can provide useful information to further experimental investigations.

DOI: 10.1103/PhysRevD.94.074012

I. INTRODUCTION

Heavy-light mesons composed of one heavy quark and one light quark act as the hydrogen atoms of hadron physics and are the ideal laboratory for the understanding of strong interactions in the nonperturbative regime [1–3]. In the past several years, significant progress has been achieved in studying the charmed and charmed-strange states experimentally [4–8]. It is widely accepted that the ground charmed and charmed-strange mesons such as $D(1S)$, $D(1P)$, $D_s(1S)$, and $D_s(1P)$ have been established [4], and some candidates for higher radial and orbital excitations have also been reported, which have stimulated many theoretical investigations on these excitations [9–28].

Recently, the LHCb Collaboration studied $B^+\pi^-$ and $B^0\pi^-$ invariant mass distributions by analysing pp collision data at center-of-mass energies of 7 and 8 TeV [29]. Precise masses and widths of the $B_1(5721)$ and $B_2^*(5747)$ are measured, and two excited bottom mesons $B_J(5840)^{0,+}$ and $B_J(5960)^{0,+}$ are observed, whose masses and widths are also studied with various quantum number hypotheses. The measured masses and widths of the neutral $B_J(5840)$ and $B_J(5960)$ under different spin-parity hypotheses are listed in Table I. In 2013, the CDF Collaboration studied the $B^0\pi^+$ and $B^+\pi^-$ invariant mass distributions using the data from $p\bar{p}$ collisions at $\sqrt{s} = 1.96$ TeV [30]. A new resonance $B(5970)$ is found both in the $B^0\pi^+$ and $B^+\pi^-$ mass distributions, and the mass and with of the neutral $B(5970)$ are $5978 \pm 5 \pm 12$ MeV and $70^{+30}_{-20} \pm 30$ MeV, respectively. Since the $B(5970)$ can decay into $B\pi$ final state, it should be a natural spin-parity state.

Unlike the prosperity of charm sector, experimental information on excited bottom and bottom-strange mesons is scarce. Therefore, the above excited B mesons reported by the LHCb and CDF Collaborations provide a good platform to study the low-lying excited bottom and bottom-strange mesons. Some theoretical predictions on masses and widths of bottom and bottom-strange mesons have been performed in different approaches such as constituent quark model [31–35], chiral quark model [11], $^3P_0$ model [36–38], heavy meson effective theory [39,40], and other approaches [41,42]. These theoretical predictions are not completely consistent with each other. In order to understand the natures of the $B_J(5840)$, $B_J(5960)$, and $B(5970)$, further test calculations against the experimental measurements are required.

The main purpose of this work is to discuss the possible quark-model assignments of the $B_J(5840)$, $B_J(5960)$, and $B(5970)$. We shall calculate the masses of excited bottom and bottom-strange mesons in a nonrelativistic quark model and the corresponding strong decay behaviors in the $^3P_0$ model. The relevant radiative transitions are also evaluated.

This work is organized as follows. In Sec. II, we calculate the bottom and bottom-strange meson masses in a nonrelativistic quark model. In Sec. III, we evaluate the two-body Okubo-Zweig-Iizuka (OZI)-allowed strong decays of the bottom and bottom-strange mesons in the $^3P_0$ model with the realistic wave functions from the quark model employed in Sec. II. In Sec. IV, we give the $E1$ and $M1$ radiative decays of the bottom and bottom-strange mesons. A summary is given in the last section.

II. MASSES

To obtain the bottom and bottom-strange meson spectroscopy, we calculate the open-bottom mesons masses in a nonrelativistic quark model proposed by Lakhina and Swanson, which can describe the heavy-light meson and heavy quarkonium masses with a reasonable accuracy [43]. We have employed this model to evaluate the open-charm

*Corresponding author.
lidm@zzu.edu.cn

TABLE I. The neutral charge resonances observed by the LHCb Collaboration with different spin-parity hypotheses [29]. The N and UN stand for the natural spin parity $[P=(-1)^J]$ and unnatural spin parity $[P=(-1)^{(J+1)}]$, respectively.

Hypothesis I: Both $B_J(5840)^0$ and $B_J(5960)^0$ have UN.	
$M_{B_J(5840)^0}$	$5862.9 \pm 5.0 \pm 6.7 \pm 0.2$ MeV
$\Gamma_{B_J(5840)^0}$	$127.4 \pm 16.7 \pm 34.2$ MeV
$M_{B_J(5960)^0}$	$5969.2 \pm 2.9 \pm 5.1 \pm 0.2$ MeV
$\Gamma_{B_J(5960)^0}$	$82.3 \pm 7.7 \pm 9.4$ MeV
Hypothesis II: $B_J(5840)^0$ has N and $B_J(5960)^0$ has UN.	
$M_{B_J(5840)^0}$	$5889.7 \pm 22.0 \pm 6.7 \pm 0.2$ MeV
$\Gamma_{B_J(5840)^0}$	$107.0 \pm 19.6 \pm 34.2$ MeV
$M_{B_J(5960)^0}$	$6015.9 \pm 3.7 \pm 5.1 \pm 0.2 \pm 0.4$
$\Gamma_{B_J(5960)^0}$	$81.6 \pm 9.9 \pm 9.4$ MeV
Hypothesis III: $B_J(5840)^0$ has UN and $B_J(5960)^0$ has N.	
$M_{B_J(5840)^0}$	$5907.8 \pm 4.7 \pm 6.7 \pm 0.2 \pm 0.4$ MeV
$\Gamma_{B_J(5840)^0}$	$119.4 \pm 17.2 \pm 34.2$ MeV
$M_{B_J(5960)^0}$	$5993.6 \pm 6.4 \pm 5.1 \pm 0.2$ MeV
$\Gamma_{B_J(5960)^0}$	$55.9 \pm 6.6 \pm 9.4$ MeV

mesons masses in Ref. [18]. In this model, the total Hamiltonian can be written as

$$H = H_0 + H_{sd} + C_{q\bar{q}}, \tag{1}$$

where H_0 is the zeroth-order Hamiltonian, H_{sd} is the spin-dependent Hamiltonian, and $C_{q\bar{q}}$ is a constant. The H_0 is

$$H_0 = \frac{\boldsymbol{p}^2}{M_r} - \frac{4}{3}\frac{\alpha_s}{r} + br + \frac{32\alpha_s\sigma^3 e^{-\sigma^2 r^2}}{9\sqrt{\pi}m_q m_{\bar{q}}}\boldsymbol{S}_q\cdot\boldsymbol{S}_{\bar{q}}, \tag{2}$$

where $\boldsymbol{p}$ is the center-of-mass momentum, r is the $q\bar{q}$ separation, $M_r = 2m_q m_{\bar{q}}/(m_q + m_{\bar{q}})$; m_q and $m_{\bar{q}}$ are the masses of quark q and antiquark $\bar{q}$, respectively; $\boldsymbol{S}_q$ and $\boldsymbol{S}_{\bar{q}}$ are the spins of the quark q and antiquark $\bar{q}$, respectively. The spin-dependent part H_{sd} can be expressed as

$$\begin{aligned} H_{sd} = {} & \left(\frac{\boldsymbol{S}_q}{2m_q^2} + \frac{\boldsymbol{S}_{\bar{q}}}{2m_{\bar{q}}^2}\right)\cdot\boldsymbol{L}\left(\frac{1}{r}\frac{dV_c}{dr} + \frac{2}{r}\frac{dV_1}{dr}\right) \\ & + \frac{\boldsymbol{S}_+\cdot\boldsymbol{L}}{m_q m_{\bar{q}}}\left(\frac{1}{r}\frac{dV_2}{r}\right) \\ & + \frac{3\boldsymbol{S}_q\cdot\hat{\boldsymbol{r}}\boldsymbol{S}_{\bar{q}}\cdot\hat{\boldsymbol{r}} - \boldsymbol{S}_q\cdot\boldsymbol{S}_{\bar{q}}}{3m_q m_{\bar{q}}}V_3 \\ & + \left[\left(\frac{\boldsymbol{S}_q}{m_q^2} - \frac{\boldsymbol{S}_{\bar{q}}}{m_{\bar{q}}^2}\right) + \frac{\boldsymbol{S}_-}{m_q m_{\bar{q}}}\right]\cdot\boldsymbol{L}V_4, \end{aligned} \tag{3}$$

where $\boldsymbol{L}$ is the relative orbital angular momentum of the $q\bar{q}$ system, and

$$\begin{aligned} V_c &= -\frac{4}{3}\frac{\alpha_s}{r} + br, \\ V_1 &= -br - \frac{2}{9\pi}\frac{\alpha_s^2}{r}[9\ln(\sqrt{m_q m_{\bar{q}}}r) + 9\gamma_E - 4], \\ V_2 &= -\frac{4}{3}\frac{\alpha_s}{r} - \frac{1}{9\pi}\frac{\alpha_s^2}{r}[-18\ln(\sqrt{m_q m_{\bar{q}}}r) \\ &\quad + 54\ln(\mu r) + 36\gamma_E + 29], \\ V_3 &= -\frac{4\alpha_s}{r^3} - \frac{1}{3\pi}\frac{\alpha_s^2}{r^3}[-36\ln(\sqrt{m_q m_{\bar{q}}}r) \\ &\quad + 54\ln(\mu r) + 18\gamma_E + 31], \\ V_4 &= \frac{1}{\pi}\frac{\alpha_s^2}{r^3}\ln\left(\frac{m_{\bar{q}}}{m_q}\right), \\ \boldsymbol{S}_\pm &= \boldsymbol{S}_q \pm \boldsymbol{S}_{\bar{q}}. \end{aligned} \tag{4}$$

Here $\gamma_E = 0.5772$ and the scale μ is set to 1.1 GeV.

The parameters used in this work are $\alpha_s = 0.5$, $b = 0.14$ GeV^2, $\sigma = 1.17$ GeV, $C_{d\bar{b}} = 0.003$ GeV, $C_{s\bar{b}} = 0.051$ GeV. The constituent quark masses are taken to be $m_u = m_d = 0.45$ GeV, $m_s = 0.55$ GeV, and $m_b = 4.5$ GeV.

The spin-orbit term included in the H_{sd} can be decomposed into symmetric part $H_{\rm sym}$ and antisymmetric part $H_{\rm anti}$. These two parts can be written as

$$\begin{aligned} H_{\rm sym} = {} & \frac{\boldsymbol{S}_+\cdot\boldsymbol{L}}{2}\left[\left(\frac{1}{2m_q^2} + \frac{1}{2m_{\bar{q}}^2}\right)\left(\frac{1}{r}\frac{dV_c}{dr} + \frac{2}{r}\frac{dV_1}{dr}\right)\right. \\ & \left. + \frac{2}{m_q m_{\bar{q}}}\left(\frac{1}{r}\frac{dV_2}{r}\right) + \left(\frac{1}{m_q^2} - \frac{1}{m_{\bar{q}}^2}\right)V_4\right], \end{aligned} \tag{5}$$

$$\begin{aligned} H_{\rm anti} = {} & \frac{\boldsymbol{S}_-\cdot\boldsymbol{L}}{2}\left[\left(\frac{1}{2m_q^2} - \frac{1}{2m_{\bar{q}}^2}\right)\left(\frac{1}{r}\frac{dV_c}{dr} + \frac{2}{r}\frac{dV_1}{dr}\right)\right. \\ & \left. + \left(\frac{1}{m_q^2} + \frac{1}{m_{\bar{q}}^2} + \frac{2}{m_q m_{\bar{q}}}\right)V_4\right]. \end{aligned} \tag{6}$$

The antisymmetric part $H_{\rm anti}$ gives rise to the spin-orbit mixing of the heavy-light mesons with different total spins but with the same total angular momentum such as $B(n^3L_L)$ and $B(n^1L_L)$ [$B_s(n^3L_L)$ and $B_s(n^1L_L)$]. Hence, the two physical states $B_L(nL)$ and $B'_L(nL)$ [$B_{sL}(nL)$ and $B'_{sL}(nL)$] can be expressed as [12,31,44]

$$\begin{pmatrix} B_L(nL) \\ B'_L(nL) \end{pmatrix} = \begin{pmatrix} \cos\theta_{nL} & \sin\theta_{nL} \\ -\sin\theta_{nL} & \cos\theta_{nL} \end{pmatrix}\begin{pmatrix} B(n^1L_L) \\ B(n^3L_L) \end{pmatrix}, \tag{7}$$

$$\begin{pmatrix} B_{sL}(nL) \\ B'_{sL}(nL) \end{pmatrix} = \begin{pmatrix} \cos\theta'_{nL} & \sin\theta'_{nL} \\ -\sin\theta'_{nL} & \cos\theta'_{nL} \end{pmatrix}\begin{pmatrix} B_s(n^1L_L) \\ B_s(n^3L_L) \end{pmatrix}, \tag{8}$$

where the θ_{nL} and θ'_{nL} are the mixing angles. The $B'_L(nL)$ [$B'_{sL}(nL)$] refers to the higher mass state.

With the help of Mathematica program [45], we solve the Schrödinger equation with Hamiltonian H_0 and treat the H_{sd}

TABLE II. The B meson masses in MeV from different quark models. The mixing angles of $B_L - B'_L$ obtained in this work are $\theta_{1P} = -34.6°$, $\theta_{2P} = -36.1°$, $\theta_{1D} = -39.6°$, $\theta_{2D} = -39.7°$, $\theta_{1F} = -41.0°$. Dots indicates that the corresponding mass was not calculated in the corresponding reference.

State	This work	ZVR [32]	DE [33]	EFG [34]	LNR [35]
$B(1^1S_0)$	5280	5280	5279	5280	5277
$B(1^3S_1)$	5329	5330	5324	5326	5325
$B(2^1S_0)$	5910	5830	5886	5890	5822
$B(2^3S_1)$	5939	5870	5920	5906	5848
$B(3^1S_0)$	6369	6210	6320	6379	6117
$B(3^3S_1)$	6391	6240	6347	6387	6136
$B(1^3P_0)$	5683	5650	5706	5749	5678
$B_1(1P)$	5729	5690	5700	5723	5686
$B'_1(1P)$	5754	5690	5742	5774	5699
$B(1^3P_2)$	5768	5710	5714	5741	5704
$B(2^3P_0)$	6145	6060	6163	6221	6010
$B_1(2P)$	6185	6100	6175	6209	6022
$B'_1(2P)$	6241	6100	6194	6281	6028
$B(2^3P_2)$	6253	6120	6188	6260	6040
$B(1^3D_1)$	6095	5970	6025	6119	6005
$B_2(1D)$	6004	5960	5985	6103	5920
$B'_2(1D)$	6113	5980	6037	6121	5955
$B(1^3D_3)$	6014	5970	5993	6091	5871
$B(2^3D_1)$	6497	⋯	⋯	6534	6248
$B_2(2D)$	6435	6310	⋯	6528	6179
$B'_2(2D)$	6513	6320	⋯	6554	6207
$B(2^3D_3)$	6444	6320	⋯	6542	6140
$B(1^3F_2)$	6383	6190	6264	6412	⋯
$B_3(1F)$	6236	6180	6220	6391	⋯
$B'_3(1F)$	6393	6200	6271	6420	⋯
$B(1^3F_4)$	6243	6180	6226	6380	⋯

TABLE III. The B_s meson masses in MeV from different quark models. The mixing angles of $B_{sL} - B'_{sL}$ obtained in this work are $\theta'_{1P} = -34.9°$, $\theta'_{2P} = -36.1°$, $\theta'_{1D} = -39.8°$, $\theta'_{2D} = -39.8°$, $\theta'_{1F} = -41.1°$. Dots indicates that the corresponding mass was not calculated in the corresponding reference.

State	This work	ZVR [32]	DE [33]	EFG [34]	LNR [35]
$B_s(1^1S_0)$	5362	5370	5373	5372	5366
$B_s(1^3S_1)$	5413	5430	5421	5414	5417
$B_s(2^1S_0)$	5977	5930	5985	5976	5939
$B_s(2^3S_1)$	6003	5970	6019	5992	5966
$B_s(3^1S_0)$	6415	6310	6421	6467	6254
$B_s(3^3S_1)$	6435	6340	6449	6475	6274
$B_s(1^3P_0)$	5756	5750	5804	5833	5781
$B_{s1}(1P)$	5801	5790	5805	5831	5795
$B'_{s1}(1P)$	5836	5800	5842	5865	5805
$B_s(1^3P_2)$	5851	5820	5820	5842	5815
$B_s(2^3P_0)$	6203	6170	6264	6318	6143
$B_{s1}(2P)$	6241	6200	6278	6321	6153
$B'_{s1}(2P)$	6297	6210	6296	6345	6160
$B_s(2^3P_2)$	6309	6220	6292	6359	6170
$B_s(1^3D_1)$	6142	6070	6127	6209	6094
$B_{s2}(1D)$	6087	6070	6095	6189	6043
$B'_{s2}(1D)$	6159	6080	6140	6218	6067
$B_s(1^3D_3)$	6096	6080	6103	6191	6016
$B_s(2^3D_1)$	6527	⋯	⋯	6629	6362
$B_{s2}(2D)$	6492	6410	⋯	6625	6320
$B'_{s2}(2D)$	6542	6420	⋯	6651	6339
$B_s(2^3D_3)$	6500	6420	⋯	6637	6298
$B_s(1^3F_2)$	6412	6300	6369	6501	⋯
$B_{s3}(1F)$	6313	6280	6332	6468	⋯
$B'_{s3}(1F)$	6422	6310	6376	6515	⋯
$B_s(1^3F_4)$	6319	6290	6337	6475	⋯

as the perturbative term. The obtained bottom and bottom-strange meson masses are shown in Tables II and III. The predictions of some other quark models [32–35] are also listed.

It is believed that the $q\bar{q}$ system can be described by the relativistic Hamiltonian

$$H = \sqrt{p^2 + m_q^2} + \sqrt{p^2 + m_{\bar{q}}^2} + V(r). \tag{9}$$

For the heavy quarkonium, because of p being smaller than the quark mass, the kinetic energy terms in Eq. (9) can be expanded in inverse powers of the quark mass to obtain the nonrelativistic Hamiltonian. The heavy-light meson state is in principle a relativistic system since p is not smaller than the light constituent quark mass m. Therefore, it is necessary to discuss the applicability of the nonrelativistic approximation for the relativistic heavy-light system. It is suggested that the following Martin's operator bound is valid for arbitrary mass M [46]:

$$\sqrt{p^2 + m^2} \leq \frac{M}{2} + \frac{p^2}{2M} + \frac{m^2}{2M}. \tag{10}$$

This equation gives an upper limit of the relativistic kinetic energy term. The equality in Eq. (10) holds if the extremum is taken in M. Based on this effective mass expansion of the relativistic kinetic energy term, Jaczko and Durand explain the success of Martin's nonrelativistic descriptions for the spectra of the relativistic light-light and heavy-light mesons [47]. In fact, when an extremum is taken already in the spectrum, the resulting procedure is just a variational method, which establishes a connection between the nonrelativistic potential model and the relativistic potential model. This method, based on the original work [48] and also known as the auxiliary or einbein field method, has proven to be rather accurate in various calculations for the relativistic systems [49] and has been applied to the light-light and heavy-light mesons, glueballs, and hybrids [49–55]. This suggests that one can describe the relativistic heavy-light mesons with formally nonrelativistic formulas.

When we discuss the possible assignments of the observed bottom states based on the mass information, we use the mass ranges from different quark models including the nonrelativistic and relativistic models rather than only from the nonrelativistic model (1).

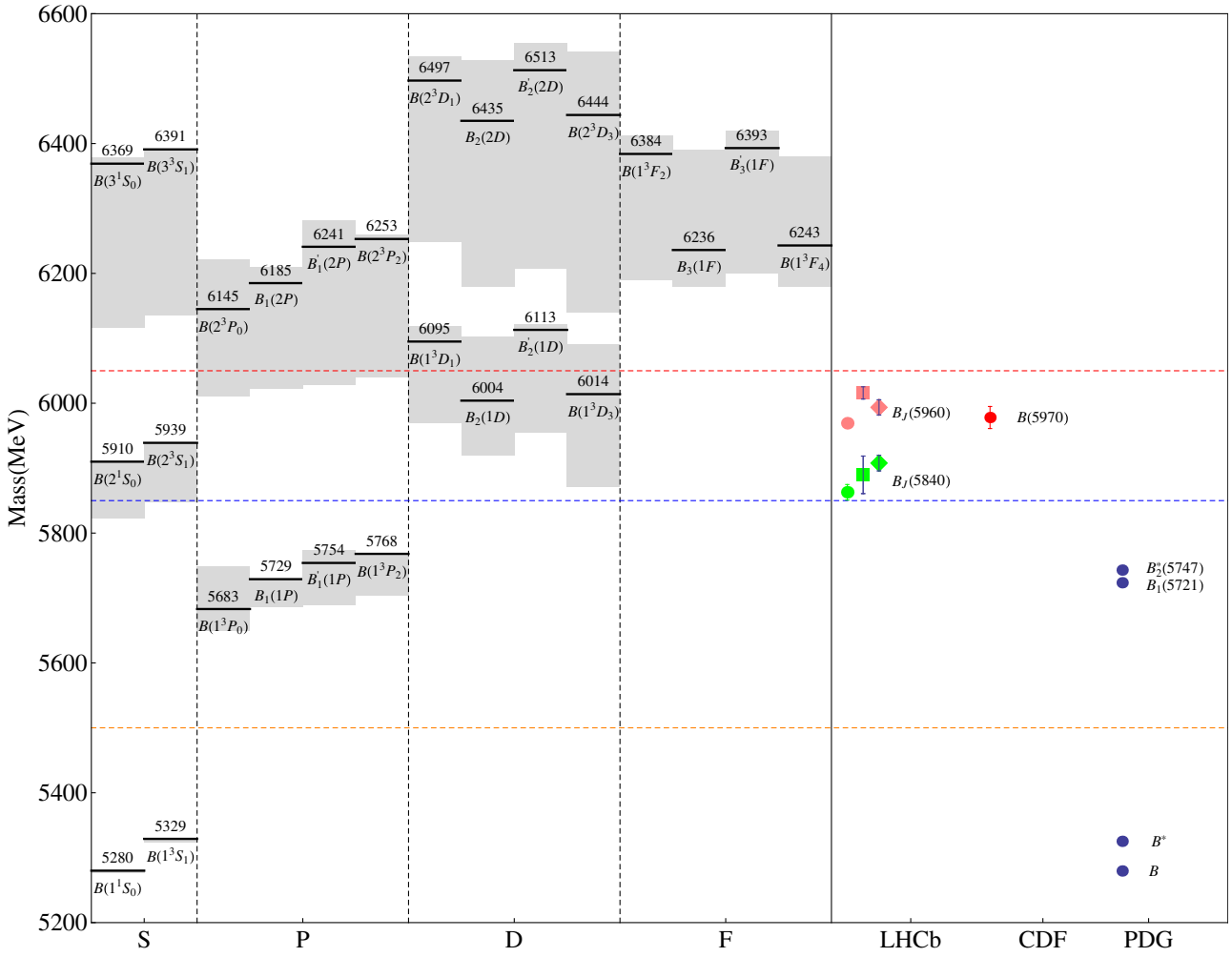

FIG. 1. The bottom meson spectrum. The solid lines stand for our predictions and the shaded regions are the expected mass ranges from some other quark models [32–35]. The observed bottom states are also depicted. The N and UN denote natural parity and unnatural parity, respectively.

The predicted mass ranges from different quark models and the observed bottom states are shown in Fig. 1. It is shown that the ground states B and B^* can be well described. For the P wave bottom mesons, $B_1(5721)$ and $B_2^*(5747)$ lie within the $1P$ mass range. Hence, the $B_1(5721)$ can be regarded as the $B_1(1P)$ or $B_1'(1P)$, and the $B_2^*(5747)$ is identified as the $B(1^3P_2)$. The observed $B_J(5840)$, $B_J(5960)$, and $B(5970)$ lie close to the mass ranges of the $B(2^1S_0)$, $B(2^3S_1)$, $B_2(1D)$, and $B(1^3D_3)$ states. Considering the spin parity and masses, we tentatively identify the $B(5970)$ as the $B(2^3S_1)$ or $B(1^3D_3)$ state. For the $B_J(5840)$ and $B_J(5960)$, all spin-parity hypotheses should be considered. The bottom-strange mesons B_s and B_s^* are well established. The $B_{s1}(5830)$ and $B_{s2}^*(5840)$ can be clarified into P wave bottom-strange mesons. The assignments for these observed bottom and bottom-strange states are listed in Table IV. Below, we shall focus on these possible assignments. Since the mass information alone is insufficient to identify these states, the strong decay behaviors also need to be investigated in the $^3P_0$ model.

TABLE IV. Possible assignments for the observed bottom and bottom-strange states based on masses and spin parity.

State	Possible Assignments
$B_1(5721)$	$B_1(1P)$, $B_1'(1P)$
$B_2^*(5747)$	$B(1^3P_2)$
$B(5970)$	$B(2^3S_1)$, $B(1^3D_3)$
$B_J(5840)$UN	$B(2^1S_0)$
$B_J(5960)$UN	$B_2(1D)$
$B_J(5840)$N	$B(2^3S_1)$
$B_J(5960)$UN	$B_2(1D)$
$B_J(5840)$UN	$B(2^1S_0)$
$B_J(5960)$N	$B(2^3S_1)$, $B(1^3D_3)$
$B_{s1}(5830)$	$B_{s1}(1P)$, $B_{s1}'(1P)$
$B_{s2}^*(5840)$	$B_s(1^3P_2)$

III. STRONG DECAYS

A. $^3P_0$ model

In this work, we adopt the $^3P_0$ model to evaluate the Okubo-Zweig-Iizuka-allowed two-body strong decays of the bottom and bottom-strange mesons. The $^3P_0$ model, also called as quark pair creation model, has been widely applied to study hadron strong decays with considerable success [56–59]. In this model, the meson decay occurs through a quark-antiquark pair with the vacuum quantum number [60]. Here we give a brief review of the $^3P_0$ model. The transition operator T of the decay $A \to BC$ in the $^3P_0$ model can be written as [61]

$$T = -3\gamma\sum_m \langle 1m1-m|00\rangle \int d^3\boldsymbol{p}_3 d^3\boldsymbol{p}_4 \delta^3(\boldsymbol{p}_3+\boldsymbol{p}_4) \times \mathcal{Y}_1^m\left(\frac{\boldsymbol{p}_3-\boldsymbol{p}_4}{2}\right)\chi^{34}_{1-m}\phi_0^{34}\omega_0^{34}b_3^\dagger(\boldsymbol{p}_3)d_4^\dagger(\boldsymbol{p}_4), \quad (11)$$

where γ is a dimensionless $q_3\bar{q}_4$ pair-production strength, and $\boldsymbol{p}_3$ and $\boldsymbol{p}_4$ are the momenta of the created quark q_3 and antiquark $\bar{q}_4$, respectively. ϕ_0^{34}, ω_0^{34}, and $\chi^{34}_{1,-m}$ are the flavor, color, and spin wave functions of the $q_3\bar{q}_4$, respectively. The solid harmonic polynomial $\mathcal{Y}_1^m(\boldsymbol{p}) \equiv |p|^1 Y_1^m(\theta_p,\phi_p)$ reflects the momentum-space distribution of the $q_3\bar{q}_4$.

The partial wave amplitude $\mathcal{M}^{LS}(\boldsymbol{P})$ can be expressed as

$$\mathcal{M}^{LS}(\boldsymbol{P}) = \sum_{M_{J_B},M_{J_C},M_S,M_L} \langle LM_L SM_S|J_AM_{J_A}\rangle \times \langle J_BM_{J_B}J_CM_{J_C}|SM_S\rangle \times \int d\Omega Y^*_{LM_L}\mathcal{M}^{M_{J_A}M_{J_B}M_{J_C}}(\boldsymbol{P}), \quad (12)$$

where $\mathcal{M}^{M_{J_A}M_{J_B}M_{J_C}}(\boldsymbol{P})$ is the helicity amplitude and defined as

$$\langle BC|T|A\rangle = \delta^3(\boldsymbol{P}_A-\boldsymbol{P}_B-\boldsymbol{P}_C)\mathcal{M}^{M_{J_A}M_{J_B}M_{J_C}}(\boldsymbol{P}). \quad (13)$$

The $|A\rangle$, $|B\rangle$, and $|C\rangle$ denote the mock meson states and the mock meson $|A\rangle$ is defined by [62]

$$|A(n_A^{2S_A+1}L_{AJ_AM_{J_A}})(\boldsymbol{P}_A)\rangle \equiv \sqrt{2E_A}\sum_{M_{L_A},M_{S_A}}\langle L_AM_{L_A}S_AM_{S_A}|J_AM_{J_A}\rangle \times \int d^3\boldsymbol{p}_A\psi_{n_AL_AM_{L_A}}(\boldsymbol{p}_A)\chi^{12}_{S_AM_{S_A}}\phi_A^{12}\omega_A^{12} \times \left|q_1\left(\frac{m_1}{m_1+m_2}\boldsymbol{P}_A+\boldsymbol{p}_A\right)\bar{q}_2\left(\frac{m_2}{m_1+m_2}\boldsymbol{P}_A-\boldsymbol{p}_A\right)\right\rangle,$$

where m_1 and m_2 ($\boldsymbol{p}_1$ and $\boldsymbol{p}_2$) are the masses (momenta) of the quark q_1 and the antiquark $\bar{q}_2$, respectively; $\boldsymbol{P}_A = \boldsymbol{p}_1+\boldsymbol{p}_2$, $\boldsymbol{p}_A = \frac{m_2\boldsymbol{p}_1-m_1\boldsymbol{p}_2}{m_1+m_2}$; $\chi^{12}_{S_AM_{S_A}}$, ϕ_A^{12}, ω_A^{12}, $\psi_{n_AL_AM_{L_A}}(\boldsymbol{p}_A)$ are the spin, flavor, color, and space wave functions of the meson A composed of $q_1\bar{q}_2$ with total energy E_A, respectively.

Because of different choices of the pair-production vertex, the phase space conventions, and the employed meson wave functions, various $^3P_0$ models exist in literatures. In this work, we restrict to the simplest vertex as introduced originally by [60], which assumes a spatially constant pair-production strength γ, adopt the relativistic phase space as Ref. [61], and employ the realistic meson wave functions from the quark model (1). With the relativistic phase space, the decay width $\Gamma(A\to BC)$ can be expressed in terms of the partial wave amplitude Eq. (12)

$$\Gamma(A\to BC) = \frac{\pi P}{4M_A^2}\sum_{LS}|\mathcal{M}^{LS}(\boldsymbol{P})|^2, \quad (14)$$

where $P = |\boldsymbol{P}| = \frac{\sqrt{[M_A^2-(M_B+M_C)^2][M_A^2-(M_B-M_C)^2]}}{2M_A}$, and M_A, M_B, and M_C are the masses of the mesons A, B, and C, respectively.

We take the light nonstrange quark pair creation strength $\gamma = 7.6$ by fitting to the total width of the $B_2^*(5747)$ as the $B(1^3P_2)$ state. The γ and strange quark pair creation strength $\gamma_{s\bar{s}}$ can be related by $\gamma_{s\bar{s}} = \gamma\frac{m_u}{m_s}$ [63], where the constituent quark masses m_u and m_s are the same as those used in the mass estimates in the quark model (1). Our value of γ is higher than that used by other groups such as [22,59] by a factor of $\sqrt{96\pi}$ due to different field conventions. The mixing angles θ_{nL} are taken from Tables II and III.

B. $B(1P)$ states

For the $B(1^3P_0)$ state, the predicted mass is above the $B\pi$ threshold. The decay widths of the $B(1^3P_0)$ are shown in Table V. No experimental data of the $B(1^3P_0)$ exist, but some theoretical estimations also give a broad width [9,36], which is consistent with our result.

In Table VI, we give the decay widths of the $B_2^*(5747)$. The γ-independent ratio is predicted to be

TABLE V. Decay widths of the $B(1^3P_0)$ in MeV.

$B^+\pi^-$	153.80
$B^0\pi^0$	76.62
Total width	230.43

TABLE VI. Decay widths of the $B_2^*(5747)$ in MeV.

$B^+\pi^-$	8.46
$B^0\pi^0$	4.16
$B^{*+}\pi^-$	7.97
$B^{*0}\pi^0$	3.92
Total width	24.51
Experiment	$24.5 \pm 1.0 \pm 11.5$

TABLE VII. Decay widths of the $B_1(5721)$ in MeV.

Channel	$B_1(1P)$	$B_1'(1P)$
$B^{*+}\pi^-$	132.77	27.12
$B^{*0}\pi^0$	66.63	13.51
Total width	199.40	40.63
Experiment	$30.1 \pm 1.5 \pm 3.5$	

$$\frac{\Gamma(B_2^*(5747)^0 \to B^* + \pi^-)}{\Gamma(B_2^*(5747)^0 \to B^+\pi^-)} = 0.95, \tag{15}$$

which is consistent with experimental data of $1.10 \pm 0.42 \pm 0.31$ [64] and $0.71 \pm 0.14 \pm 0.30$ [29].

The decay widths of the $B_1(5721)$ as the $B_1(1P)$ and $B_1'(1P)$ are listed in Table VII. With the $B_1(1P)$ assignment to the $B_1(5721)$, the total decay width is expected to be about 200 MeV, much larger than the experiment, hence this assignment can be totally excluded. With the $B_1'(1P)$ assignment, the total width of the $B_1(5721)$ is 40.63 MeV, consistent with $30.1 \pm 1.5 \pm 3.5$ given by the LHCb Collaboration [29].

The dependence of the $B_1(5721)$ total width on the mixing angle θ_{1P} is depicted in Fig 2. The predicted mixing angle from the quark model (1) is $\theta_{1P} = -34.6°$. With this angle, the $B_1(1P)$ decay width is much broader than that of the $B_1'(1P)$, which is consistent with other theoretical predictions [9,36]. In the heavy quark effective theory, the P wave heavy-light mesons can be divided into the $(0^+, 1^+)_{j=\frac{1}{2}}$ and $(1^+, 2^+)_{j=\frac{3}{2}}$ doublets, where j is the total angular momentum of the light quark. In the heavy quark limit, the $\theta_{1P} = -54.7°$, which is close to quark-model prediction of $-34.6°$. For the two 1^+ states, the decay width is broader for the $j = \frac{1}{2}$ state than that for the $j = \frac{3}{2}$ state. Hence, with the $B_1'(1P)$ assignment, the $B_1(5721)$ corresponds to the 1^+ bottom meson belonging to the $(1^+, 2^+)_{j=\frac{3}{2}}$ doublets.

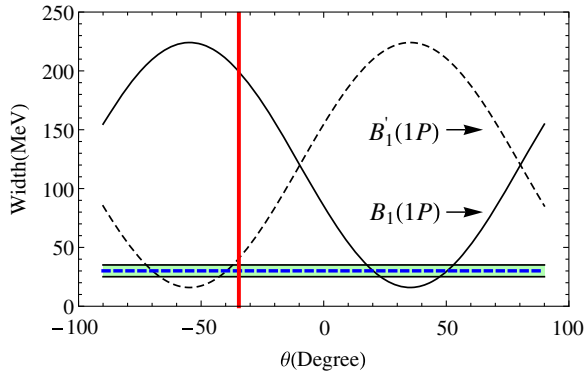

FIG. 2. Total decay width of the $B_1(5721)$ as the $B_1(1P)$ and $B_1'(1P)$ versus the mixing angle. The blue dashed line with a green band denotes the LHCb experimental data. The vertical red solid line corresponds to the mixing angle $\theta_{1P} = -34.6°$ obtained in Sec. II.

C. $B_J(5840)$ and $B_J(5960)$

For the $B_J(5840)$ and $B_J(5960)$, three spin-parity hypotheses exist, which classifies these states into different possible assignments. In the following, we will consider these assignments one by one.

In Table VIII, we list the decay widths of the $B_J(5840)$ and $B_J(5960)$ under the hypothesis I. The predicted total width of the $B_J(5840)$ as the $B(2^1S_0)$ is 126.22 MeV, in good agreement with the experimental data of $127.4 \pm 16.7 \pm 34.2$ MeV. However, the predicted total width of the $B_J(5960)$ as the $B_2(1D)$ is much larger than the experimental data of $82.3 \pm 7.7 \pm 9.4$ MeV.

The predicted decay widths of the $B_J(5840)$ and $B_J(5960)$ under the hypothesis II are presented in Table IX. The predicted total width of the $B_J(5840)$ as the $B(2^3S_1)$ state is 106.13 MeV, consistent with the experimental data of $107.0 \pm 19.7 \pm 34.2$ MeV. However, the predicted total width of the $B_J(5960)$ as the $B_2(1D)$ state is much larger than the experimental data of $81.6 \pm 9.9 \pm 9.4$ MeV.

The decay widths of the $B_J(5840)$ and $B_J(5960)$ under the hypothesis III are shown in Table X. The predicted width of the $B_J(5840)$ as the $B(2^1S_0)$ is about 134 MeV, consistent with the measured result of $119.4 \pm 17.2 \pm 34.2$ MeV. If the $B_J(5960)$ is the $B(2^3S_1)$, the $B_J(5960)$ total width is expected to be 131.97 MeV, far away from the measured width of $55.9 \pm 6.6 \pm 9.4$ MeV. If the $B_J(5960)$ is the $B(1^3D_3)$, the $B_J(5960)$ total width is expected to be 48.55 MeV, in good agreement with the data of $55.9 \pm 6.6 \pm 9.4$ MeV.

To sum up, with the hypothesis III, the total widths of the $B_J(5840)$ and $B_J(5960)$ can be reproduced simultaneously. The strong decay behaviors combined with masses indicate that the $B_J(5840)$ and $B_J(5960)$ can be identified as the $B(2^1S_0)$ and $B(1^3D_3)$, respectively. The assignment

TABLE VIII. Decay widths of the $B_J(5840)$ and $B_J(5960)$ under the hypothesis I in MeV. Dots indicate that a decay mode is forbidden.

	$B_J(5840)$ $B(2^1S_0)$	$B_J(5960)$ $B_2(1D)$
$B^{*+}\pi^-$	84.13	63.51
$B^{*0}\pi^0$	42.09	31.83
$B(1^3P_0)^+\pi^-$	⋯	69.62
$B(1^3P_0)^0\pi^0$	⋯	34.61
$B_2^*(5747)^+\pi^-$	⋯	0.005
$B_2^*(5747)^0\pi^0$	⋯	0.002
$B_1(1P)^+\pi^-$	⋯	0.01
$B_1(1P)^0\pi^0$	⋯	0.005
$B_1'(1P)^+\pi^-$	⋯	0.17
$B_1'(1P)^+\pi^-$	⋯	0.08
$B^*\eta$	⋯	11.41
B_s^*K	⋯	10.98
Total width	126.22	222.24
Experiment	$127.4 \pm 16.7 \pm 34.2$	$82.3 \pm 7.7 \pm 9.4$

TABLE IX. Decay widths of the $B_J(5840)$ and $B_J(5960)$ under the hypothesis II in MeV. Dots indicate that a decay mode is forbidden.

	$B_J(5840)$ $B(2^3S_1)$	$B_J(5960)$ $B_2(1D)$
$B^+\pi^-$	20.43	⋯
$B^0\pi^0$	10.26	⋯
$B^{*+}\pi^-$	46.68	59.21
$B^{*0}\pi^0$	23.39	29.70
$B(1^3P_0)^+\pi^-$	0.002	84.63
$B(1^3P_0)^0\pi^0$	2.9×10^{-4}	42.42
$B_2^*(5747)^+\pi^-$	⋯	0.01
$B_2^*(5747)^0\pi^0$	⋯	0.006
$B_1(1P)^+\pi^-$	0.21	0.05
$B_1(1P)^0\pi^0$	0.10	0.02
$B_1'(1P)^+\pi^-$	0.05	0.54
$B_1'(1P)^+\pi^-$	0.02	0.26
$B\eta$	2.61	⋯
$B^*\eta$	0.98	16.79
B_sK	1.40	⋯
B_s^*K	⋯	24.14
Total width	106.13	257.79
Experiment	$107.0\pm19.6\pm34.2$	$81.6\pm9.9\pm9.4$

of the $B_J(5840)$ as the $B(2^1S_0)$ state is also suggested by the LHCb Collaboration [29]. The main decay modes of the $B(2^1S_0)$ are expected to $B^*\pi$ and $B^*\eta$. The main decay modes of the $B(1^3D_3)$ are expected to be $B\pi$ and $B^*\pi$.

TABLE X. Decay widths of the $B_J(5840)$ and $B_J(5960)$ under the hypothesis III in MeV. Dots indicate that a decay mode is forbidden.

	$B_J(5840)$	$B_J(5960)$	
	$B(2^1S_0)$	$B(2^3S_1)$	$B(1^3D_3)$
$B^+\pi^-$	⋯	14.39	15.08
$B^0\pi^0$	⋯	7.25	7.48
$B^{*+}\pi^-$	86.24	38.20	16.17
$B^{*0}\pi^0$	43.21	19.20	8.03
$B^{*+}(1^3P_0)\pi^-$	4.1×10^{-4}	⋯	⋯
$B^{*0}(1^3P_0)\pi^0$	4.0×10^{-5}	⋯	⋯
$B_2^*(5747)^+\pi^-$	0.05	1.62	0.35
$B_2^*(5747)^0\pi^0$	0.02	0.76	0.16
$B_1(1P)^+\pi^-$	⋯	0.37	0.15
$B_1(1P)^0\pi^0$	⋯	0.18	0.07
$B_1'(1P)^+\pi^-$	⋯	2.41	0.04
$B_1'(1P)^+\pi^-$	⋯	1.14	0.02
$B\eta$	⋯	6.74	0.44
$B^*\eta$	4.57	12.06	0.23
B_sK	⋯	11.81	0.26
B_s^*K	⋯	15.83	0.08
Total width	134.09	131.97	48.55
Experiment	$119.4\pm17.2\pm34.2$	$55.9\pm6.6\pm9.4$	

TABLE XI. Decay widths of the $B(5970)$ as the $B(2^3S_1)$ and $B(1^3D_3)$ in MeV.

	$B(5970)$	
	$B(2^3S_1)$	$B(1^3D_3)$
$B^+\pi^-$	15.54	13.496
$B^0\pi^0$	7.83	6.69
$B^{*+}\pi^-$	40.26	14.26
$B^{*0}\pi^0$	20.23	7.08
$B_2^*(5747)^+\pi^-$	1.02	0.21
$B_2^*(5747)^0\pi^0$	0.47	0.10
$B_1(1P)^+\pi^-$	0.31	0.10
$B_1(1P)^0\pi^0$	0.15	0.05
$B_1'(1P)^+\pi^-$	1.63	0.02
$B_1'(1P)^+\pi^-$	0.77	0.12
$B\eta$	6.38	0.31
$B^*\eta$	10.66	0.14
B_sK	10.35	0.16
B_s^*K	12.12	0.03
Total width	127.72	42.69
Experiment	$70^{+30}_{-20}\pm30$	

D. $B(5970)$

The decay widths of the $B(5970)$ as the $B(2^3S_1)$ and $B(1^3D_3)$ are listed in Table XI. Since the $B(5970)$ mass is close to the $B_J(5960)$ mass, the results for the $B(2^3S_1)$ and $B(1^3D_3)$ are similar with those in Table X. However, because of the large uncertainty of the $B(5970)$ total width, both the $B(2^3S_1)$ and $B(1^3D_3)$ assignments are favored by the experimental data [30]. Reference [36] interprets the $B(5870)$ as the $B(2^3S_1)$ state while Ref. [9] assigns the $B(5970)$ as the $B(1^3D_3)$ state [9]. The main decay modes of the $B(2^3S_1)$ are expected to be $B\pi$, $B^*\pi$, $B\eta$, $B^*\eta$, B_sK, and B_s^*K, while the $B(1^3D_3)$ is expected to mainly decay to $B\pi$, $B^*\pi$. Further precise measurements of the width, spin and decay modes are needed to distinguish these two assignments.

E. $B(1^3D_1)$, $B_2(1D)$ and $B_2'(1D)$

Given the bottom masses and spin parity, no experimental candidates exist for the $B(1^3D_1)$, $B_2(1D)$ and $B_2'(1D)$ states. Our predicted masses for these three states are 6095, 6004, and 6113 MeV, respectively. With these masses as inputs, their total decay widths are listed in Table XII.

It is shown that all these three states have large total widths more than 200 MeV. The decay modes of these states are different, mainly due to the quantum number conservation and the threshold.

In heavy quark limit, the mixing angle is $\theta_{1D}=-50.8°$ [65]. Our predicted $\theta_{1D}=-39.6°$ is close to $-50.8°$. With this mixing angle, the total decay width of the $B_2(1D)$ is broader than that of the $B_2'(1D)$, which indicate that the

TABLE XII. Decay widths of the $B(1^3D_1)$, $B_2(1D)$ and $B_2'(1D)$ states in MeV. Dots indicate that a decay mode is forbidden.

	$B(1^3D_1)$	$B_2(1D)$	$B_2'(1D)$
$B^+\pi^-$	26.44	...	...
$B^0\pi^0$	13.31	...	...
$B^{*+}\pi^-$	15.45	60.57	61.08
$B^{*0}\pi^0$	7.76	30.38	30.44
$B(1^3P_0)^+\pi^-$	4.52	81.79	3.51
$B(1^3P_0)^0\pi^0$	2.21	40.93	1.76
$B_2^*(5747)^+\pi^-$	...	0.01	0.20
$B_2^*(5747)^0\pi^0$	...	0.005	0.10
$B_1(1P)^+\pi^-$	10.30	0.03	0.18
$B_1(1P)^0\pi^0$	5.20	0.02	0.09
$B_1'(1P)^+\pi^-$	74.77	0.42	5.57
$B_1'(1P)^+\pi^-$	37.71	0.20	2.74
$B\eta$	14.18	...	...
$B^*\eta$	7.34	15.58	4.64
B_sK	32.67	...	...
B_s^*K	15.06	20.75	5.04
$B^+\rho^-$	10.64	...	48.37
$B^0\rho^0$	5.27	...	24.04
$B^{*+}\rho^-$	...	...	4.02
$B^{*0}\rho^0$	...	...	2.01
$B\omega$	4.20	...	21.08
$B^*\omega$	...	...	0.58
$B(2^1S_0)^+\pi^-$	0.52	...	...
$B(2^1S_0)^0\pi^0$	0.24	...	...
$B(2^3S_1)^+\pi^-$	0.05	...	0.01
$B(2^3S_1)^0\pi^0$	0.02	...	0.01
Total width	287.85	250.69	215.47

$B_2(1D)$ and $B_2'(1D)$ correspond to the $(1^-, 2^-)_{j=\frac{3}{2}}$ and $(2^-, 3^-)_{j=\frac{5}{2}}$ doublets, respectively.

F. $B_s(1P)$ states

For the $B_s(1^3P_0)$ state, the predicted mass is below the BK threshold, which is consistent with some other studies [32,66]. Hence, there is no OZI-allowed strong decay pattern and the dominant decay mode may be $B_s\pi$. This situation is analogous to the charmed-strange partner $D_{s0}^*(2317)$, whose decay width is mainly due to OZI-violated $D_s\pi$ channel. Based on higher mass of the $B_s(1^3P_0)$ state, some theoretical calculations give a broad decay width [9,36]. Further experimental search for the $B_s(1^3P_0)$ state will distinguish these two predictions.

The decay widths of the $B_{s2}^*(5840)$ are listed in Table XIII. The predicted total decay width is 1.99 MeV, in good agreement with LHCb experimental data of $1.56 \pm 0.13 \pm 0.47$ MeV [4,67] and the CDF result of $1.4 \pm 0.4 \pm 0.2$ MeV [30]. The predicted ratio

$$\frac{\Gamma(B_{s2}^*(5840) \to B^{*+}K^-)}{\Gamma(B_{s2}^*(5840) \to B^+K^-)} = 0.086 \qquad (16)$$

TABLE XIII. Decay widths of the $B_{s2}^*(5840)$ in MeV.

B^+K^-	1.00
$B^0\bar{K}^0$	0.86
$B^{*+}K^-$	0.09
$B^{*0}\bar{K}^0$	0.05
Total width	1.99
Experiment	$1.56 \pm 0.13 \pm 0.47/1.4 \pm 0.4 \pm 0.2$

is independent with the γ and in agreement with the LHCb experimental data of $0.093 \pm 0.013 \pm 0.012$ [4,67].

In analogous to the $B_1(5721)$, the $B_{s1}(5830)$ can be the $B_{s1}(1P)$ or $B_{s1}'(1P)$. With the predicted mixing angle $\theta_{1P} = -34.9°$, the total widths of the $B_{s1}(1P)$ and $B_{s1}'(1P)$ are expected to be 162.76 and 21.35 MeV, respectively, both much larger than the CDF data of $0.5 \pm 0.3 \pm 0.3$ MeV [30]. The dependence of the total widths of $B_{s1}(1P)$ and $B_{s1}'(1P)$ states versus the mixing angle are shown in Fig 3. It can be seen that when the mixing angle varies in the range of $(-59.2 \sim -50.4)°$, the total width of the $B_{s1}(1P)$ is consistent with the observed width. In the heavy quark effective theory, the ideal value of the mixing angle is $\theta_{1P} = -54.7°$,

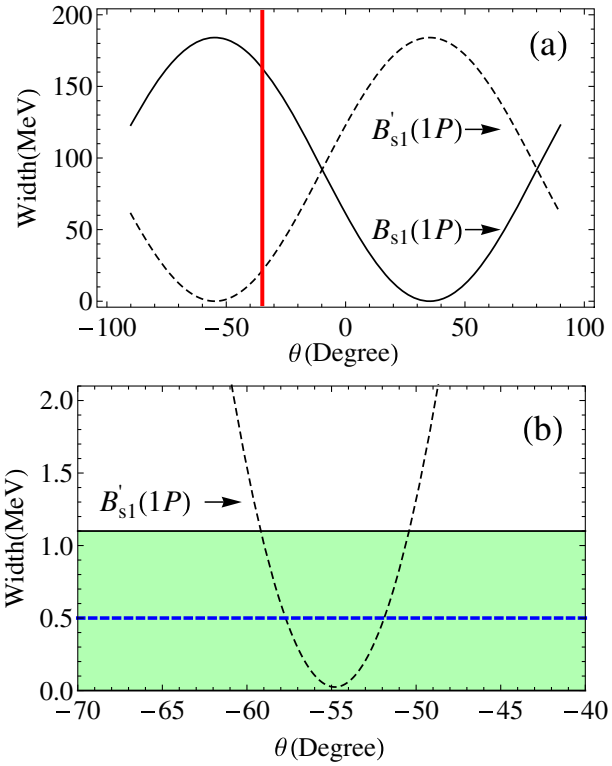

FIG. 3. (a) Total width of the $B_{s1}(5830)$ as the $B_{s1}(1P)$ and $B_{s1}'(1P)$ versus the mixing angle. The vertical red solid line corresponds to the mixing angle $\theta_{1P} = -34.9°$ obtained in Sec. II. (b) The variation of total width of the $B_{s1}'(1P)$ with mixing angle $\theta_{1P} = (-70 \sim -40)°$. The blue dashed line with a green band denotes the CDF experimental data.

TABLE XIV. Decay widths of the $B_s(2^1S_0)$ and $B_s(2^3S_1)$ in MeV.

	$B_s(2^1S_0)$	$B_s(2^3S_1)$
B^+K^-	⋯	35.67
$B^0\bar{K}^0$	⋯	35.67
$B^{*+}K^-$	106.62	70.71
$B^{*0}\bar{K}^0$	105.26	70.29
$B_s\eta$	⋯	5.32
$B_s^*\eta$	1.51	4.24
Total width	213.38	221.90

lying in the range of $(-59.2 \sim -50.4)°$. The extremely narrow total width of the $B_{s1}(5830)$ suggests that it can be identified as the $B'_{s1}(1P)$ state belonging to the $(1^+, 2^+)_{j=\frac{3}{2}}$ doublet.

G. $B_s(2S)$

Our predicted masses of the $B_s(2^1S_0)$ and $B_s(2^3S_1)$ are 5977 and 6003 MeV, respectively. The decay widths of the $B_s(2^1S_0)$ and $B_s(2^3S_1)$ are listed in Table XIV. It is shown that the $B_s(2^1S_0)$ state mainly decays into B^*K, and the main decay modes of the $B_s(2^3S_1)$ state are BK and B^*K.

H. $B_s(1^3D_1)$, $B_s(1^3D_3)$, $B_{s2}(1D)$, $B'_{s2}(1D)$

Our predicted masses of the $B_s(1^3D_1)$, $B_s(1^3D_3)$, $B_{s2}(1D)$, $B'_{s2}(1D)$ are 6142, 6096, 6087, and 6159 MeV, respectively. The decay widths of these states are shown in Table XV. The $B_s(1^3D_1)$ state is expected to be broad, while the $B_s(1^3D_3)$ is a narrow state. This behavior is similar with their bottom partners $B(1^3D_1)$ and $B(1^3D_3)$. The dominant decay modes of the $B_s(1^3D_1)$ and $B_s(1^3D_3)$ are BK and B^*K.

The mixing angle of the $B_{s2}(1D)$ and $B'_{s2}(1D)$ states is expected to be $-39.8°$, close to the ideal mixing angle $-50.8°$ in the heavy quark limit. For the $B_{s2}(1D)$ and $B'_{s2}(1D)$, the B^*K channel is expected to be the dominant decay mode. The broad $B_{s2}(1D)$ and the narrow $B'_{s2}(1D)$ correspond to the 2^- bottom-strange mesons belonging to the $(1^-, 2^-)_{j=\frac{3}{2}}$ and $(1^-, 2^-)_{j=\frac{5}{2}}$ doublets, respectively.

TABLE XV. Decay widths of the $B_s(1D)$ states in MeV.

	$B_s(1^3D_1)$	$B_s(1^3D_3)$	$B_{s2}(1D)$	$B'_{s2}(1D)$
B^+K^-	52.95	11.99	⋯	⋯
$B^0\bar{K}^0$	53.48	11.70	⋯	⋯
$B^{*+}K^-$	29.36	11.04	90.12	38.53
$B^{*0}\bar{K}^0$	29.57	10.74	90.38	37.88
$B_s\eta$	19.13	0.57	⋯	⋯
$B_s^*\eta$	8.80	0.30	18.15	2.95
Total width	213.38	46.33	198.64	79.37

IV. RADIATIVE TRANSITIONS

Besides the strong decays, the radiative transitions are also the important tools to determine the properties of heavy-light mesons. We evaluate the $E1$ and $M1$ radiative partial widths between the $v = n^{2S+1}L_J$ and $v' = n'^{2S'+1}L'_{J'}$ states using [22,68,69]

$$\Gamma_{E1}(v \to v' + \gamma) = \frac{4\alpha e_Q^2}{3} C_{fi}\delta_{SS'}|\langle v'|r|v\rangle|^2 \frac{E_\gamma^3 E_f}{M_i}, \quad (17)$$

$$\Gamma_{M1}(v \to v' + \gamma) = \frac{\alpha e_Q'^2}{3}\frac{2J'+1}{2L+1}\delta_{LL'}\delta_{SS'\pm 1}\left|\langle v'|j_0\left(\frac{E_\gamma r}{2}\right)|v\rangle\right|^2 \frac{E_\gamma^3 E_f}{M_i}, \quad (18)$$

where $e_Q = \frac{m_q Q_b + m_b Q_q}{m_q + m_b}$, $e'_Q = \frac{m_q Q_b + m_b Q_q}{m_q m_b}$, Q_b and Q_q stand for the charges of the quark b and q in units of $|e|$, respectively. $\alpha = 1/137$ is the fine-structure constant, E_γ is the photon energy, E_f is the energy of final heavy-light meson, M_i is the mass of initial state, and the angular matrix element C_{fi} can be expressed as

$$C_{fi} = \mathrm{Max}(L, L')(2J'+1)\begin{Bmatrix} L' & J' & S \\ J & L & 1 \end{Bmatrix}^2. \quad (19)$$

The wave functions obtained from the quark model (1) are used to calculate the $E1$ and $M1$ radiative partial widths. To determine the photon and final state energies, the masses of these initial and final states should be involved. For the well established B, B^*, B_s, and B_s^*, the masses are taken from PDG [4]. For the $B'_1(1P)$, $B(1^3P_2)$, $B(2^1S_0)$, $B(1^3D_3)$, $B'_{s1}(1P)$, and $B_s(1^3P_2)$, their masses are taken to be the $B_1(5721)$, $B_2^*(5747)$, $B_J(5840)$, $B_J(5960)$, $B_{s1}(5830)$, and $B_{s2}^*(5840)$ masses, respectively. For other states, their masses are taken from the predictions of the quark model (1). The $E1$ and $M1$ transitions widths of the neutral charge open-bottom states together with the photon energies are listed in Tables XVI, XVII, XVIII, and XIX.

From Table XVI, it can be seen that the $B(1^3P_0)\gamma$, $B_1(1P)\gamma$, and $B'_1(1P)\gamma$ channels are essential to discriminate the $B(2^3S_1)$ and $B(1^3D_3)$ interpretations for the B (5970), since these decay mode are forbidden for the $B(1^3D_3)$ state while allowable for the $B(2^3S_1)$ state. The $B(1^3P_2)\gamma$ final state for these two assignments has sizable decay widths, and can be observed experimentally.

TABLE XVI. E1 transitions widths of neutral charge bottom mesons. E_γ in MeV and Γ in keV.

Multiplets	Initial Meson	Final Meson	E_γ	Γ
$B(2S) \to B(1P)$	$B(2^3S_1)$	$B(1^3P_0)$	250	21.4
	$B(2^3S_1)$	$B(1^3P_2)$	196	51.6
	$B(2^3S_1)$	$B_1(1P)$	206	11.67
	$B(2^3S_1)$	$B_1'(1P)$	210	25.9
	$B(2^1S_0)$	$B_1(1P)$	176	49.6
	$B(2^1S_0)$	$B_1'(1P)$	180	25.2
$B(1P) \to B(1S)$	$B(1^3P_0)$	$B(1^3S_1)$	347	116.9
	$B(1^3P_2)$	$B(1^3S_1)$	400	177.7
	$B_1(1P)$	$B(1^3S_1)$	390	53.1
	$B_1'(1P)$	$B(1^3S_1)$	386	108.5
	$B_1(1P)$	$B(1^1S_0)$	432	130.2
	$B_1'(1P)$	$B(1^1S_0)$	428	60.4
$B(1D) \to B(1P)$	$B(1^3D_3)$	$B(1^3P_2)$	248	127.0
	$B(1^3D_1)$	$B(1^3P_2)$	345	9.3
	$B(1^3D_1)$	$B(1^3P_0)$	398	283.5
	$B(1^3D_1)$	$B_1(1P)$	355	49.0
	$B(1^3D_1)$	$B_1'(1P)$	359	106.2
	$B_2(1D)$	$B(1^3P_2)$	258	14.5
	$B_2(1D)$	$B_1(1P)$	269	143.1
	$B_2(1D)$	$B_1'(1P)$	273	0.1
	$B_2'(1D)$	$B(1^3P_2)$	362	57.2
	$B_2'(1D)$	$B_1(1P)$	372	8.6
	$B_2'(1D)$	$B_1'(1P)$	376	356.3

TABLE XVII. E1 transitions widths of the neutral charge bottom-strange mesons. E_γ in MeV and Γ in keV.

Multiplets	Initial Meson	Final Meson	E_γ	Γ
$B_s(2S) \to B_s(1P)$	$B_s(2^3S_1)$	$B_s(1^3P_0)$	242	17.2
	$B_s(2^3S_1)$	$B_s(1^3P_2)$	161	25.6
	$B_s(2^3S_1)$	$B_{s1}(1P)$	199	9.4
	$B_s(2^3S_1)$	$B_{s1}'(1P)$	172	12.6
	$B_s(2^1S_0)$	$B_{s1}(1P)$	173	41.7
	$B_s(2^1S_0)$	$B_{s1}'(1P)$	146	12.3
$B_s(1P) \to B_s(1S)$	$B_s(1^3P_0)$	$B_s(1^3S_1)$	330	84.7
	$B_s(1^3P_2)$	$B_s(1^3S_1)$	409	159
	$B_{s1}(1P)$	$B_s(1^3S_1)$	372	39.5
	$B_{s1}'(1P)$	$B_s(1^3S_1)$	398	98.8
	$B_{s1}(1P)$	$B_s(1^1S_0)$	418	97.7
	$B_{s1}'(1P)$	$B_s(1^1S_0)$	444	56.6
$B_s(1D) \to B_s(1P)$	$B_s(1^3D_3)$	$B_s(1^3P_2)$	251	113.2
	$B_s(1^3D_1)$	$B_s(1^3P_2)$	295	5.1
	$B_s(1^3D_1)$	$B_s(1^3P_0)$	374	204.4
	$B_s(1^3D_1)$	$B_{s1}(1P)$	332	35.3
	$B_s(1^3D_1)$	$B_{s1}'(1P)$	305	56.8
	$B_{s2}(1D)$	$B_s(1^3P_2)$	242	10.5
	$B_{s2}(1D)$	$B_{s1}(1P)$	279	138.8
	$B_{s2}(1D)$	$B_{s1}'(1P)$	253	0.04
	$B_{s2}'(1D)$	$B_s(1^3P_2)$	311	31.5
	$B_{s2}'(1D)$	$B_{s1}(1P)$	348	5.9
	$B_{s2}'(1D)$	$B_{s1}'(1P)$	321	195.4

TABLE XVIII. M1 transitions widths of the neutral charge bottom mesons. E_γ in MeV and Γ in keV.

Initial Multiplet	Initial Meson	Final Meson	E_γ	Γ
$B(1S)$	$B(1^3S_1)$	$B(1^1S_0)$	45	0.1
$B(2S)$	$B(2^3S_1)$	$B(1^1S_0)$	623	8.0
	$B(2^3S_1)$	$B(2^1S_0)$	31	0.05
	$B(2^1S_0)$	$B(1^3S_1)$	554	0.9
$B(1P)$	$B_1(1P)$	$B(1^3P_0)$	46	0.03
	$B_1'(1P)$	$B(1^3P_0)$	42	0.01
	$B(1^3P_2)$	$B_1(1P)$	11	1.4×10^{-3}
	$B(1^3P_2)$	$B_1'(1P)$	15	1.7×10^{-3}
$B(1D)$	$B(1^3D_1)$	$B_2(1D)$	90	0.7
	$B_2'(1D)$	$B(1^3D_1)$	18	2.3×10^{-3}
	$B_2'(1D)$	$B(1^3D_3)$	118	1.4
	$B_2'(1D)$	$B_2(1D)$	108	1.9

TABLE XIX. M1 transitions widths of the neutral charge bottom-strange mesons. E_γ in MeV and Γ in keV.

Initial Multiplet	Initial Meson	Final Meson	E_γ	Γ
$B_s(1S)$	$B_s(1^3S_1)$	$B_s(1^1S_0)$	48.9	0.1
$B_s(2S)$	$B_s(2^3S_1)$	$B_s(1^1S_0)$	603	4.0
	$B_s(2^3S_1)$	$B_s(2^1S_0)$	25.9	0.02
	$B_s(2^1S_0)$	$B_s(1^3S_1)$	535	0.1
$B_s(1P)$	$B_{s1}(1P)$	$B_s(1^3P_0)$	45	0.02
	$B_{s1}'(1P)$	$B_s(1^3P_0)$	72	0.05
	$B_s(1^3P_2)$	$B_{s1}(1P)$	39	0.04
	$B_s(1^3P_2)$	$B_{s1}'(1P)$	11	5.2×10^{-4}
$B_s(1D)$	$B_s(1^3D_1)$	$B_{s2}(1D)$	55	0.1
	$B_{s2}'(1D)$	$B_s(1^3D_1)$	17	1.3×10^{-3}
	$B_{s2}'(1D)$	$B_s(1^3D_3)$	63	0.2
	$B_{s2}'(1D)$	$B_{s2}(1D)$	72	0.4

V. SUMMARY

In this paper, we calculate the bottom and bottom-strange meson spectroscopy in a nonrelativistic quark model proposed by Lakhina and Swanson. Our predictions, combined with the results from some other quark models, give the mass ranges of bottom and bottom-strange mesons. With these predictions, we give the possible quark-model assignments for these bottom mesons observed by LHCb and CDF Collaborations. Furthermore, the strong and radiative decay behaviors of these bottom and bottom-strange mesons are investigated with the realistic meson wave functions from our employed nonrelativistic quark model. The $B_1(5721)$ and $B_2^*(5747)$ can be classified into the $B_1'(1P)$ and $B(1^3P_2)$, respectively. The $B_{s1}(5830)$ and $B_{s2}^*(5840)$ can be identified as the $B_{s1}'(1P)$ and $B_s(1^3P_2)$ states, respectively. The $B_J(5840)$ and $B_J(5960)$ can be explained as the $B(2^1S_0)$ and $B(1^3D_3)$, respectively. The $B(5970)$ can be interpreted as the $B(2^3S_1)$ or $B(1^3D_3)$. The properties of other states are also predicted, which will be helpful to search for these states experimentally.

ACKNOWLEDGMENTS

We would like to thank Tim Gershon from the LHCb Collaboration and Yu-Bing Dong from IHEP for valuable discussions. This work is partly supported by the National Natural Science Foundation of China under Grant No. 11505158, the China Postdoctoral Science Foundation under Grant No. 2015M582197, the Postdoctoral Research Sponsorship in Henan Province under Grant No. 2015023, and the Startup Research Fund of Zhengzhou University (Grants No. 1511317001 and No. 1511317002).

[1] A. De Rujula, H. Georgi, and S. L. Glashow, Charm Spectroscopy via Electron-Positron Annihilation, Phys. Rev. Lett. **37**, 785 (1976).
[2] J. L. Rosner, P-Wave Mesons with One Heavy Quark, Comments Nucl. Part. Phys. **16**, 109 (1986).
[3] S. Godfrey and J. Napolitano, Light meson spectroscopy, Rev. Mod. Phys. **71**, 1411 (1999).
[4] K. A. Olive *et al.* (Particle Data Group Collaboration), Review of Particle Physics, Chin. Phys. C **38**, 090001 (2014).
[5] R. Aaij *et al.* (LHCb Collaboration), Observation of Overlapping Spin-1 and Spin-3 $\bar{D}^0K^-$ Resonances at Mass 2.86 GeV/c^2, Phys. Rev. Lett. **113**, 162001 (2014).
[6] R. Aaij *et al.* (LHCb Collaboration), Dalitz plot analysis of $B_s^0 \to \bar{D}^0K^-\pi^+$ decays, Phys. Rev. D **90**, 072003 (2014).
[7] R. Aaij *et al.* (LHCb Collaboration), First observation and amplitude analysis of the $B^- \to D^+K^-\pi^-$ decay, Phys. Rev. D **91**, 092002 (2015).
[8] R. Aaij *et al.* (LHCb Collaboration), Dalitz plot analysis of $B^0 \to \bar{D}^0\pi^+\pi^-$ decays, Phys. Rev. D **92**, 032002 (2015).
[9] X. H. Zhong and Q. Zhao, Strong decays of heavy-light mesons in a chiral quark model, Phys. Rev. D **78**, 014029 (2008).
[10] X. H. Zhong, Strong decays of the newly observed $D(2550)$, $D(2600)$, $D(2750)$, and $D(2760)$, Phys. Rev. D **82**, 114014 (2010).
[11] L. Y. Xiao and X. H. Zhong, Strong decays of higher excited heavy-light mesons in a chiral quark model, Phys. Rev. D **90**, 074029 (2014).
[12] Q. F. Lü and D. M. Li, Understanding the charmed states recently observed by the LHCb and *BABAR* Collaborations in the quark model, Phys. Rev. D **90**, 054024 (2014).
[13] Z. G. Wang, Analysis of strong decays of the charmed mesons $D(2550)$, $D(2600)$, $D(2750)$ and $D(2760)$, Phys. Rev. D **83**, 014009 (2011).
[14] P. Colangelo, F. De Fazio, F. Giannuzzi, and S. Nicotri, New meson spectroscopy with open charm and beauty, Phys. Rev. D **86**, 054024 (2012).
[15] Z. G. Wang, Analysis of strong decays of the charmed mesons $D_J(2580)$, $D_J^*(2650)$, $D_J(2740)$, $D_J^*(2760)$, $D_J(3000)$, $D_J^*(3000)$, Phys. Rev. D **88**, 114003 (2013).
[16] Z. G. Wang, $D_{s3}^*(2860)$ and $D_{s1}^*(2860)$ as the 1D $c\bar{s}$ states, Eur. Phys. J. C **75**, 25 (2015).
[17] Z. F. Sun, J. S. Yu, X. Liu, and T. Matsuki, Newly observed $D(2550)$, $D(2610)$, and $D(2760)$ as $2S$ and $1D$ charmed mesons, Phys. Rev. D **82**, 111501 (2010).
[18] D. M. Li, P. F. Ji, and B. Ma, The newly observed open-charm states in quark model, Eur. Phys. J. C **71**, 1582 (2011).
[19] Y. Sun, X. Liu, and T. Matsuki, Newly observed $D_J(3000)^{+,0}$ and $D_J^*(3000)^0$ as $2P$ states in D meson family, Phys. Rev. D **88**, 094020 (2013).
[20] Q. T. Song, D. Y. Chen, X. Liu, and T. Matsuki, $D_{s1}^*(2860)$ and $D_{s3}^*(2860)$: Candidates for $1D$ charmed-strange mesons, Eur. Phys. J. C **75**, 30 (2015).
[21] Q. T. Song, D. Y. Chen, X. Liu, and T. Matsuki, Charmed-strange mesons revisited: Mass spectra and strong decays, Phys. Rev. D **91**, 054031 (2015).
[22] F. E. Close and E. S. Swanson, Dynamics and decay of heavy-light hadrons, Phys. Rev. D **72**, 094004 (2005).
[23] S. Godfrey and K. Moats, $D_{sJ}^*(2860)$ mesons as excited D-wave $c\bar{s}$ states, Phys. Rev. D **90**, 117501 (2014).
[24] J. Segovia, D. R. Entem, and F. Fernndez, Scaling of the $^3P_0$ strength in heavy meson strong decays, Phys. Lett. B **715**, 322 (2012).
[25] J. Segovia, D. R. Entem, and F. Fernandez, Charmed-strange meson spectrum: Old and new problems, Phys. Rev. D **91**, 094020 (2015).
[26] Z. Y. Zhou and Z. Xiao, Hadron loops effect on mass shifts of the charmed and charmed-strange spectra, Phys. Rev. D **84**, 034023 (2011).
[27] B. Chen, L. Yuan, and A. Zhang, Possible 2S and 1D charmed and charmed-strange mesons, Phys. Rev. D **83**, 114025 (2011).
[28] Z. H. Wang, G. L. Wang, J. M. Zhang, and T. H. Wang, The productions and strong decays of $D_q(2S)$ and $B_q(2S)$, J. Phys. G **39**, 085006 (2012).
[29] R. Aaij *et al.* (LHCb Collaboration), Precise measurements of the properties of the $B_1(5721)^{0,+}$ and $B_2^*(5747)^{0,+}$ states and observation of $B^{+,0}\pi^{-,+}$ mass structures, J. High Energy Phys. 04 (2015) 024.
[30] T. A. Aaltonen *et al.* (CDF Collaboration), Study of orbitally excited B mesons and evidence for a new $B\pi$ resonance, Phys. Rev. D **90**, 012013 (2014).
[31] S. Godfrey and N. Isgur, Mesons in a relativized quark model with chromodynamics, Phys. Rev. D **32**, 189 (1985).
[32] J. Zeng, J. W. Van Orden, and W. Roberts, Heavy mesons in a relativistic model, Phys. Rev. D **52**, 5229 (1995).
[33] M. Di Pierro and E. Eichten, Excited heavy-light systems and hadronic transitions, Phys. Rev. D **64**, 114004 (2001).
[34] D. Ebert, R. N. Faustov, and V. O. Galkin, Heavy-light meson spectroscopy and Regge trajectories in the relativistic quark model, Eur. Phys. J. C **66**, 197 (2010).

[35] T. A. Lahde, C. J. Nyfalt, and D. O. Riska, Spectra and M1 decay widths of heavy light mesons, Nucl. Phys. **A674**, 141 (2000).
[36] Y. Sun, Q. T. Song, D. Y. Chen, X. Liu, and S. L. Zhu, Higher bottom and bottom-strange mesons, Phys. Rev. D **89**, 054026 (2014).
[37] Z. G. Luo, X. L. Chen, and X. Liu, $B_{s1}(5830)$ and $B_{s2} * (5840)$, Phys. Rev. D **79**, 074020 (2009).
[38] J. Ferretti and E. Santopinto, Open-flavor strong decays of open-charm and open-bottom mesons in the $^3P_0$ pair-creation model, arXiv:1506.04415.
[39] H. Xu, X. Liu, and T. Matsuki, Newly observed $B(5970)$ and the predictions of its spin and strange partners, Phys. Rev. D **89**, 097502 (2014).
[40] Z. G. Wang, Strong decays of the bottom mesons $B_1(5721)$, $B_2(5747)$, $B_{s1}(5830)$, $B_{s2}(5840)$ and $B(5970)$, Eur. Phys. J. Plus **129**, 186 (2014).
[41] P. Gelhausen, A. Khodjamirian, A. A. Pivovarov, and D. Rosenthal, Radial excitations of heavy-light mesons from QCD sum rules, Eur. Phys. J. C **74**, 2979 (2014).
[42] Z. G. Wang, Strong decay of the heavy tensor mesons with QCD sum rules, Eur. Phys. J. C **74**, 3123 (2014).
[43] O. Lakhina and E. S. Swanson, A xanonical $D_s(2317)$?, Phys. Lett. B **650**, 159 (2007).
[44] S. Godfrey and R. Kokoski, Properties of p-wave mesons with one heavy quark, Phys. Rev. D **43**, 1679 (1991).
[45] W. Lucha and F. F. Schoberl, Solving the Schrodinger equation for bound states with Mathematica 3.0, Int. J. Mod. Phys. C **10**, 607 (1999).
[46] A. Martin, Collapse of systems of relativistic particles, Phys. Lett. B **214**, 561 (1988).
[47] G. Jaczko and L. Durand, Understanding the success of nonrelativistic potential models for relativistic quark-antiquark bound states, Phys. Rev. D **58**, 114017 (1998).
[48] L. Brink, P. Di Vecchia, and P. S. Howe, A Lagrangian formulation of the classical and quantum dynamics of spinning particles, Nucl. Phys. **B118**, 76 (1977).
[49] Y. S. Kalashnikova, A. V. Nefediev, and Y. A. Simonov, QCD string in light-light and heavy-light mesons, Phys. Rev. D **64**, 014037 (2001).
[50] Y. A. Simonov, Regge trajectories from QCD, Phys. Lett. B **226**, 151 (1989).
[51] Y. S. Kalashnikova and Y. B. Yufryakov, Hybrid excitations of the QCD string with quarks, Phys. Lett. B **359**, 175 (1995).
[52] A. B. Kaidalov and Y. A. Simonov, Glueball masses and Pomeron trajectory in nonperturbative QCD approach, Phys. Lett. B **477**, 163 (2000).
[53] Y. S. Kalashnikova and A. V. Nefediev, Orbitally excited D and B mesons in the approach of the QCD string with quarks at the ends, Phys. Lett. B **530**, 117 (2002).
[54] Y. A. Simonov, Dynamics of confined gluons, Phys. At. Nucl. **68**, 1294 (2005); Yad. Fiz. **68**, 1347 (2005).
[55] F. Buisseret and C. Semay, On two- and three-body descriptions of hybrid mesons, Phys. Rev. D **74**, 114018 (2006).
[56] A. Le Yaouanc, L. Oliver, O. Pene, and J. C. Raynal, *Hadron Transitions in the Quark Model* (Gordon and Breach, New York, 1988).
[57] W. Roberts and B. Silverstr-Brac, General method of calculation of any hadronic decay in the p wave triplet model, Few-Body Syst. **11**, 171 (1992).
[58] H. G. Blundell, Ph.D. thesis, Carleton Universtiy, 1996 [arXiv:hep-ph/9608473].
[59] E. S. Ackleh, T. Barnes, and E. S. Swanson, On the mechanism of open flavor strong decays, Phys. Rev. D **54**, 6811 (1996); T. Barnes, F. E. Close, P. R. Page, and E. S. Swanson, Higher quarkonia, Phys. Rev. D **55**, 4157 (1997); T. Barnes, N. Black, and P. R. Page, Strong decays of strange quarkonia, Phys. Rev. D **68**, 054014 (2003).
[60] L. Micu, Decay rates of meson resonances in a quark model, Nucl. Phys. **B10**, 521 (1969).
[61] D. M. Li and B. Ma, $X(1835)$ and $\eta(1760)$ observed by BES the Collaboration, Phys. Rev. D **77**, 074004 (2008); $\eta(2225)$ observed by the BES Collaboration, Phys. Rev. D **77**, 094021 (2008); D. M. Li and E. Wang, Canonical interpretation of the $\eta_2(1870)$, Eur. Phys. J. C **63**, 297 (2009).
[62] C. Hayne and N. Isgur, Beyond the wave function at the origin: Some momentum dependent effects in the non-relativistic quark model, Phys. Rev. D **25**, 1944 (1982).
[63] A. Le Yaouanc, L. Oliver, O. Pene, and J. C. Raynal, Why is $\psi(4.414)$ so narrow?, Phys. Lett. B **72B**, 57 (1977).
[64] V. M. Abazov *et al.* (D0 Collaboration), Observation and Properties of $L = 1B_1$ and B_2^* Mesons, Phys. Rev. Lett. **99**, 172001 (2007).
[65] R. N. Cahn and J. D. Jackson, Spin-orbit and tensor forces in heavy quark light quark mesons: Implications of the new D_s state at 2.32-GeV, Phys. Rev. D **68**, 037502 (2003); T. Matsuki, T. Morii, and K. Seo, Mixing angle between $^3P_1$ and $^1P_1$ in HQET, Prog. Theor. Phys. **124**, 285 (2010).
[66] H. Y. Cheng and F. S. Yu, Near mass degeneracy in the scalar meson sector: Implications for $B^*_{(s)0}$ and $B'_{(s)1}$ mesons, Phys. Rev. D **89**, 114017 (2014).
[67] R. Aaij *et al.* (LHCb Collaboration), First Observation of the Decay $B^*_{s2}(5840)^0 \to B^{*+}K^-$ and Studies of Excited B_s^0 Mesons, Phys. Rev. Lett. **110**, 151803 (2013).
[68] S. Godfrey, Properties of the charmed P-wave mesons, Phys. Rev. D **72**, 054029 (2005).
[69] S. Godfrey, Spectroscopy of B_c mesons in the relativized quark model, Phys. Rev. D **70**, 054017 (2004).